

Quadratic Kalman Filter for Elliptical Extended Object Tracking based on Decoupling State Components

SIMON STEUERNAGEL

University of Göttingen, Göttingen, Germany

MARCUS BAUM

University of Göttingen, Göttingen, Germany

Abstract— Extended object tracking involves estimating both the physical extent and kinematic parameters of a target object, where typically multiple measurements are observed per time step. In this article, we propose a deterministic closed-form elliptical extended object tracker, based on decoupling of the kinematics, orientation, and axis lengths. By disregarding potential correlations between these state components, fewer approximations are required for the individual estimators than for an overall joint solution. The resulting algorithm outperforms existing algorithms, reaching the accuracy of sampling-based procedures. Additionally, a batch-based variant is introduced, yielding highly efficient computation while outperforming all comparable state-of-the-art algorithms. This is validated both by a simulation study using common models from literature, as well as an extensive quantitative evaluation on real automotive radar data.

Index Terms— Bayesian filtering, extended object tracking, target tracking

Manuscript received XXXXX 00, 0000; revised XXXXX 00, 0000; accepted XXXXX 00, 0000. (Corresponding author: S. Steuernagel).

Simon Steuernagel and Marcus Baum are with the Institute of Computer Science, University of Göttingen, Göttingen, 37077 Germany. (e-mail: {simon.steuernagel, marcus.baum}@cs.uni-goettingen.de).

This work has been submitted to the IEEE for possible publication. Copyright may be transferred without notice, after which this version may no longer be accessible.

Color versions of one or more of the figures in this article are available online at <http://ieeexplore.ieee.org>.

I. INTRODUCTION

TRACKING is a key technology for a wide variety of perception systems. It is employed using a range of sensor modalities, e.g., cameras, radars, or lidars. Each of these prompts its own set of challenges. Traditionally, tracked objects were often modeled as point targets, i.e., only as their position and further kinematic parameters such as velocity. However, for many applications, the physical extent, i.e., shape, of the target is of interest, for example, in order to classify the object or to perform collision avoidance. In sparse point cloud data as produced by, e.g., radar, the extent can not be easily determined using a single scan of data. Instead, information needs to be integrated over time, commonly done in a Bayesian filtering framework. This is referred to as Extended Object Tracking (EOT) [1], an example for which can be seen in Fig. 1. To track multiple extended objects [2]–[4], the state of each object must be estimated from the data. This is what this article is concerned with, i.e., the estimation of the kinematics and the extent of each individual object.

A variety of models for the target shape have been proposed. Star-convex shapes [5], [6] offer large flexibility in modeling the target extent. Even more flexibility is achieved with fully free-form approaches, such as the one recently proposed in [7]. However, one of the most common approaches in literature is to model the object extent as an ellipse [8]–[11]. The reduced size of the resulting parameter space ensures a more robust fit in sparse and noisy data, as often encountered in EOT. Furthermore, the parameterization of an ellipse and a rectangle are identical, meaning the models can often be easily transferred between the two representations.

Different concepts for tackling the problem of elliptical EOT have been proposed. By modeling the shape of the object as a Random Matrix (RM), the shape estimation can be derived in a Bayesian fashion based on the scaled sample covariance of the measurements [8], [12]. A conceptual downside of this approach is that the overall uncertainty of all shape parameters, i.e., both axes and the orientation, are represented by a single scalar value. By using variational Bayes, explicit consideration of the orientation based on the RM framework has been explored in [13].

An alternative is to model the extent based on a multiplicative factor in the measurement equation, which has been proposed in [14]. The resulting Multiplicative Error Model (MEM) forms the basis of several trackers [9], [11], [15]. Recently, [16] proposed a reinforcement learning-based tracker using it. In our previous work [15], a Rao-Blackwellized Particle Filter (RBPF) for elliptical EOT using the MEM has been derived. Numerical results show the accuracy of the tracker. However, by nature of being particle-based, it can be categorically unsuitable for specific applications, such as certain safety-critical ones. A closed-form, deterministic variant can hence be favorable.

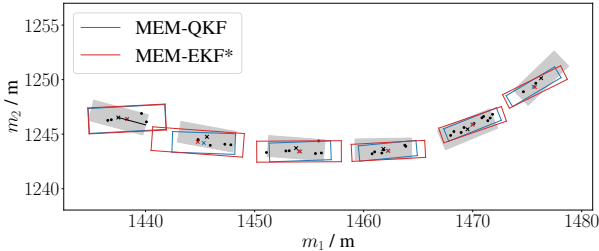


Fig. 1: Example tracking results using automotive radar data from the nuScenes data set [17]. The proposed MEM-QKF (blue) converges noticeably faster to a good estimate compared to the MEM-EKF* [9] (red), starting from the same prior (leftmost estimate). Measurements are shown as black dots, and the ground truth annotation as a gray-filled rectangle.

A. Contribution

In this article, we propose an elliptical extended object tracking algorithm, which sets a new standard for state-of-the-art closed-form trackers. To avoid approximations necessary in the derivation of the filter, we propose to treat kinematics, orientation, and size individually.

In summary, the contributions of this article are:

- 1) A deterministic, closed-form extended object tracker yielding noticeably improved results over existing closed-form methods,
- 2) a batch-based variant which achieves remarkable computational efficiency, while still matching state-of-the-art trackers in estimation accuracy,
- 3) an extensive simulation study comparing closed-form, optimization-, and sampling-based trackers,
- 4) the first large-scale, quantitative analysis comparing these methods on hundreds of trajectories of real-world automotive radar data.

This article is an extended and revised version of our conference paper [18], where the sequential measurement update was proposed. Compared to the conference version, this article adds the batch-based variant and the large-scale comparison on real-world automotive data. Besides this, the simulation study from the conference paper has been broadened, and the main body of the article has been significantly expanded.

B. Notation

Throughout this article, the superscript i denotes the measurement index, corresponding to processing measurement $\mathbf{z}_k^i, i = 1 \dots M_k$. The index $i = 0$ corresponds to the prior, and $i = M_k$ to the posterior. A superscript in brackets selects the indexed element from a vector or matrix. $\text{rot}(\cdot)$ a standard two-dimensional rotation matrix, and $\text{diag}(\cdot)$ constructs a diagonal matrix from the parameters. Analogously, $\text{blkdiag}(\cdot)$ constructs a block diagonal matrix from the input matrices.

C. Article Structure

In the following, Section II will extensively discuss existing works on the topic at hand, followed by Section III where the problem setting of the article will be defined. Next, the proposed approach will be illustrated in Section IV for the sequential and Section V for the batch-based variant. Afterwards, analysis and evaluation of the results will be presented for the simulation study in Section VI and subsequently for the experiments conducted on real-world radar data in Section VII. The article is then concluded in Section VIII.

II. RELATED WORK

A variety of previous works have tackled the problem of (elliptical) extended object tracking. In the following, these will be summarized and contrasted with the approach presented in this article.

Our proposed algorithm is based on the MEM, which was introduced in [14]. Subsequently, other approaches also based on this model will be discussed. The most prominent MEM-based tracker is the MEM-EKF*, proposed in [9]. Measurements are processed sequentially by an Extended Kalman Filter (EKF) which is specifically tailored to the problem at hand. The resulting filter can be computed in closed form. With a few additional approximations, it is possible to process a batch of measurements simultaneously, as shown in [19]. A multi-object tracker for extended objects based on [9] has been proposed in [4]. In summary, the MEM-EKF* is closely related to the proposed method, and our method could be viewed as its successor.

A different filter, working under the assumptions that the orientation can be approximated as the direction of the velocity vector was proposed in [11]. In this work, however, we are concerned with the general problem of estimating not only the kinematics and axes, but also the orientation. This problem setting is also tackled by the RBPF derived in [15], which yields significantly improved results compared to the EKF from [9]. This is achieved by accurate orientation estimation due to sampling, along with improved axis estimation by making use of the sampled orientation. However, as it is not a closed-form method, a stark conceptual difference to the method proposed here can be seen.

As discussed in Section I, an alternative modeling approach for EOT is based on random matrices. Originally proposed in [12] and further developed in [8], the method has seen widespread application. A variety of extensions have been proposed [20], e.g., incorporating the measurement number into the shape estimation [21] or incorporating physical constraints [22]. One key issue of the RM approach is the fact that the entire shape uncertainty is captured by scalar value. In particular, this means that it is not directly possible to model different process uncertainties for the axis and orientation, as needed for turning objects with fix size. A remedy has

been proposed in [13], where an iterative approach based on variational Bayes with particular focus on estimating the orientation has been proposed. Variational Bayes methods for EOT have also been explored in [23], [24], and in [25], which focused on group target tracking based on a set of ellipses, rather than a single one, as in standard elliptical EOT. Generally, these methods are not computed in closed-form, and hence are not directly comparable to the proposed approach.

In this article, we focus on the general problem of elliptical EOT, where the orientation and semi-axis lengths need to be estimated. For specific classes of tracked objects, it can make sense to instead assume correlations between the direction of the velocity and the shape orientation. Assuming these two fully coincide greatly alleviates the tracking task, which is exploited in, e.g., [10], [11]. However, it is also possible to make weaker assumptions regarding this, e.g., for drift-like behavior of targets. Such approaches can be found in [26]–[28]. Another alternative is to assume unknown but unchanging semi-axes, explored in, e.g., [29]. We focus on standard assumptions regarding the measurements, such as Gaussian measurement noise. In some applications, these assumption may not be applicable, e.g., due to heavy-tailed noise. This is treated in [30] based on an iterative variational adaption of the RM method.

III. PROBLEM SETTING

We are interested in tracking an extended object parameterized by orientation and semi-axis lengths, described at time k by the state

$$\mathbf{x}_k = [m_{1,k} \ m_{2,k} \ \dot{m}_{1,k} \ \dot{m}_{2,k} \ \theta_k \ l_{1,k} \ l_{2,k}]^T, \quad (1)$$

consisting of the kinematics \mathbf{m}_k formed jointly by position $[m_{1,k} \ m_{2,k}]^T$ and velocity $[\dot{m}_{1,k} \ \dot{m}_{2,k}]^T$, orientation θ_k , and semi-axis lengths $\mathbf{l}_k = [l_{1,k} \ l_{2,k}]^T$. Commonly, this representation is used for elliptical targets, but it can also be directly employed for rectangular ones. We do not make any assumptions on correlations between velocity and orientation as observed for specific target models, and instead treat the general case where they may be entirely independent.

In each time step, one or several measurements

$$\mathbf{z}_k^i = \mathbf{y}_k^i + \boldsymbol{\nu}_k^i \quad (2)$$

are observed. Here, the i -th noise-free measurement source \mathbf{y}_k^i at time k is uniformly distributed across the object extent and $\boldsymbol{\nu}_k^i$ is zero-mean additive noise with $\boldsymbol{\nu}_k^i \sim \mathcal{N}(0, \mathbf{R})$. We assume i.i.d. measurement noise, but all computations can be directly adapted to account for varying measurement noise between time steps or even between individual measurements of a single time step. The set of M_k measurements at time k is then given by $\mathbf{Z}_k = \{\mathbf{z}_k^i \mid i = 1 \dots M_k\}$. In certain settings, $M_k = 1 \ \forall k \in \mathbb{N}$, i.e., measurements must be processed

sequentially. In the following, this will be referred to as processing a *stream* of measurements.

This measurement setting can also be modeled using the MEM, which will be briefly reviewed in the following. The MEM gives rises to the measurement equation [14]

$$\mathbf{z}_k^i = \begin{bmatrix} m_{1,k} \\ m_{2,k} \end{bmatrix} + \text{rot}(\theta_k) \text{diag}(l_{1,k}, l_{2,k}) \begin{bmatrix} h_1 \\ h_2 \end{bmatrix} + \boldsymbol{\nu}_k^i, \quad (3)$$

i.e., the measurement source \mathbf{y}_k^i is modeled using a multiplicative term $[h_1 \ h_2]^T$. Intuitively, the term describes the relative position of the measurement source along the semi-axes of the object, which is then added to the object center position, here written explicitly without a measurement matrix. Note that this notation is equivalent to (2). The multiplicative term in (3) merely models the measurement source, but the measurement noise is still additive zero-mean Gaussian noise. The distribution of h_1 and h_2 is crucial for modeling the distribution of measurement sources on the object surface. For the previously discussed setting of uniform measurement across the full ellipse,

$$\begin{bmatrix} h_1 \\ h_2 \end{bmatrix} \sim \mathcal{N}(0, c \cdot \mathbf{I}), \quad (4)$$

with scaling factor $c = 0.25$ [9]. For a uniform distribution on a rectangle, we get $c = \frac{1}{3}$ instead. We refer to [31] for a detailed discussion on scaling factors.

The state evolves according to a discrete state transition model. For brevity, in this article, we focus on linear motion models, e.g., the constant velocity model. As discussed below, the incorporation of non-linear motion models is directly possible.

IV. METHODOLOGY

Estimating the full state from (1) jointly requires a number of approximations [9] and is commonly approached with iterative methods, e.g., variational Bayes [13]. An alternative is to decouple the state into separate components. Given a prior estimate for the individual parts, fewer approximations are needed, and more accurate individual estimators can be derived. Furthermore, such a solution gives rise to a modular algorithm, which can offer significant advantages if, e.g., complex non-linear motion models need to be incorporated.

Therefore, we decouple the full state into kinematics, orientation, and size and provide an estimator for each of the respective parts. All three components are modeled as independent random variables represented by their first two moments. The three estimates at time k for the kinematics, axis and orientation are given by $\hat{\mathbf{m}}_k$, $\hat{\mathbf{l}}_k$ and $\hat{\theta}_k$, respectively. The corresponding covariances¹ are \mathbf{P}_k^m , \mathbf{P}_k^l and \mathbf{P}_k^θ . For the update, we propose two variants of the algorithm named Multiplicative Error Model Quadratic Kalman Filter (MEM-QKF). In this section, a sequential approach will be described. Afterwards, in Section V,

¹Note that \mathbf{P}_k^θ , the variance of $\hat{\theta}_k$, is scalar, but for reasons of coherence written in the same form as the multivariate covariance matrices.

Algorithm 1: Sequential MEM-QKF

- 1) **Predict:** Compute $\hat{\mathbf{m}}_k^0, \mathbf{P}_k^{\mathbf{m},0}, \hat{\mathbf{l}}_k^0, \mathbf{P}_k^{\mathbf{l},0}, \hat{\theta}_k^0, \mathbf{P}_k^{\theta,0}$ using three standard predict steps following (5) with the corresponding process noise covariances matrices for each component.
- 2) **Update:** For each $\mathbf{z}_k^i \in \mathbf{Z}_k, i = 1 \dots |\mathbf{Z}_k|$:
 - For the update, the prior of each component is given by the posterior after processing measurement $i-1$,
 - a) Compute kinematics $\hat{\mathbf{m}}_k^i, \mathbf{P}_k^{\mathbf{m},i}$ using (6),
 - b) Compute zero-centered measurements \mathbf{s}_k^i using (9) (or (10) for $|\mathbf{Z}_k| = 1$), and pseudo-measurements using (12) and (13),
 - c) Compute axis lengths $\hat{\mathbf{l}}_k^i, \mathbf{P}_k^{\mathbf{l},i}$ using (14),
 - d) Compute orientation $\hat{\theta}_k^i, \mathbf{P}_k^{\theta,i}$ using (19),
- 3) The posterior is given by the results of the last step, i.e., $\hat{\mathbf{m}}_k^{|\mathbf{Z}_k|}, \mathbf{P}_k^{\mathbf{m},|\mathbf{Z}_k|}$ for the kinematics, $\hat{\mathbf{l}}_k^{|\mathbf{Z}_k|}, \mathbf{P}_k^{\mathbf{l},|\mathbf{Z}_k|}$ for the axis lengths, and $\hat{\theta}_k^{|\mathbf{Z}_k|}, \mathbf{P}_k^{\theta,|\mathbf{Z}_k|}$ for the orientation.

a batch-based approach which incorporates all available measurements in a single update step will be illustrated.

In this section, we follow the sequential approach taken by the original MEM-EKF* [9], processing each measurement $\mathbf{z}_k^i \in \mathbf{Z}_k$ in succession. The updates are carried out in an interleaved fashion, i.e., all three estimates are updated with \mathbf{z}_k^i before \mathbf{z}_k^{i+1} is processed. This means that the order in which the three components are updated with each new measurement does not matter. The update of each component is carried out given the estimates acquired after updating all components with the previous measurement, or with the predicted states for the first measurement.

In the following, the predict and update steps for each of the three components will be described in Sections A, C, and D. In between, the necessary pseudo-measurements for the quadratic filters used in the shape update will be introduced in Section B. A summary of the algorithm is given in Algorithm 1.

A. Kinematics

As described above, $\hat{\mathbf{m}}_k^0$ and $\mathbf{P}_k^{\mathbf{m},0}$ are given by the predicted estimate $\hat{\mathbf{m}}_{k|k-1}$ and $\mathbf{P}_{k|k-1}^{\mathbf{m}}$, acquired using the standard Kalman filter prediction step

$$\hat{\mathbf{m}}_{k|k-1} = \mathbf{F}^{\mathbf{m}} \hat{\mathbf{m}}_{k-1|k-1} , \quad (5a)$$

$$\mathbf{P}_{k|k-1}^{\mathbf{m}} = \mathbf{F}^{\mathbf{m}} \mathbf{P}_{k-1|k-1}^{\mathbf{m}} (\mathbf{F}^{\mathbf{m}})^T + \mathbf{Q}^{\mathbf{m}} , \quad (5b)$$

with $\mathbf{Q}^{\mathbf{m}}$ the covariance matrix of the additive process noise and $\mathbf{F}^{\mathbf{m}}$ the kinematic state transition matrix.

The kinematic update can be directly facilitated using the standard Kalman filter update. Given the measurement equation discussed in Section III, the distribution of an individual measurement \mathbf{z}_k^i is composed of the distribution of the measurement source on the object and the additive

noise. The update of the kinematic components reads

$$\hat{\mathbf{m}}_k^i = \hat{\mathbf{m}}_k^{i-1} + \mathbf{K}_k^i (\mathbf{z}_k^i - \mathbf{H} \hat{\mathbf{m}}_k^{i-1}) , \quad (6a)$$

$$\mathbf{P}_k^{\mathbf{m},i} = \mathbf{P}_k^{\mathbf{m},i-1} - \mathbf{K}_k^i \mathbf{H} \mathbf{P}_k^{\mathbf{m},i-1} , \quad (6b)$$

$$\mathbf{K}_k^i = \mathbf{P}_k^{\mathbf{m},i-1} \mathbf{H}^T \left(\mathbf{H} \mathbf{P}_k^{\mathbf{m},i-1} \mathbf{H}^T + \tilde{\mathbf{R}}_k \right)^{-1} . \quad (6c)$$

The measurement matrix $\mathbf{H} \in \mathbb{R}^{2 \times 4}$ selects the object center from the four-dimensional kinematic state vector. For the measurement noise $\tilde{\mathbf{R}}_k$, both the additive Gaussian noise as well as the shape of the target must be accounted for. This treats the (zero-mean) multiplicative term from (3). As discussed in [8], this is facilitated by setting

$$\tilde{\mathbf{R}}_k = \mathbf{R} + c \mathbf{X}_k , \quad (7)$$

with the shape matrix $\mathbf{X}_k \in \mathbb{R}^{2 \times 2}$ representing the object extent at time k and scaling factor c . For uniform measurements from an elliptic target, $c = 0.25$ [32], corresponding to the variance of the multiplicative term in (4). As \mathbf{X}_k is not known, we instead use the current estimate $\hat{\mathbf{X}}_k^{i-1}$ like [8], given by

$$\hat{\mathbf{x}}_k^{i-1} = \text{rot} \left(\hat{\theta}_k^{i-1} \right) \hat{\mathbf{D}}_k^{i-1} \text{rot} \left(\hat{\theta}_k^{i-1} \right)^T , \quad (8a)$$

$$\hat{\mathbf{D}}_k^{i-1} = \text{diag} \left(\left(\hat{\mathbf{l}}_k^{i-1,(1)} \right)^2, \left(\hat{\mathbf{l}}_k^{i-1,(2)} \right)^2 \right) . \quad (8b)$$

The result after computing the final measurement corresponds to the posterior estimate, i.e., $\hat{\mathbf{m}}_{k|k} = \hat{\mathbf{m}}_k^{M_k}$ and equivalent for the covariance.

B. Pseudo-Measurements

For the estimation of orientation and size, measurements are zero-centered. This is common in literature: For example, the well-established RM [8] approach updates the shape using a pseudo-measurement computed using the sample covariance of measurements. Of course, this is computed from the difference of measurements to their mean, with the mean representing an estimate for the object center. In [19], the posterior of the object center is subtracted from the measurements. In the following, we will use \mathbf{s}_k^i as the zero-centered measurements for the shape update. If more than one measurement is available at each time step, these can simply be computed as

$$\mathbf{s}_k^{i,batch} = \mathbf{z}_k^i - \bar{\mathbf{z}}_k \quad i = 1 \dots M_k , \quad (9)$$

with $\bar{\mathbf{z}}_k$ being the mean of measurements at time k . If, however, only a single measurement is received, (9) would always yield zero. As an alternative, the prior estimate of the object center $\mathbf{H} \hat{\mathbf{m}}_{k|k-1}$ can be used instead of the mean of measurements, giving rise to

$$\mathbf{s}_k^{i,stream} = \mathbf{z}_k^i - \mathbf{H} \hat{\mathbf{m}}_{k|k-1} \quad i = 1 . \quad (10)$$

This additionally introduces the uncertainty of the predicted center into the pseudo-measurement, accounted for by using

$$\mathbf{W}_k = \begin{cases} \mathbf{R}, & \text{if } M_k > 1 \\ \mathbf{R} + \mathbf{H} \mathbf{P}_{k|k-1}^{\mathbf{m}} \mathbf{H}^T, & \text{otherwise.} \end{cases} \quad (11)$$

As originally proposed in [14] and further exploited in [9], [15], we make use of quadratic pseudo-measurements for the shape update. For the axis, it is sufficient to employ

$$\mathbf{a}_k^i = \left[\left(\mathbf{s}_k^{i,(0)} \right)^2 \quad \left(\mathbf{s}_k^{i,(1)} \right)^2 \right]^T, \quad (12)$$

but for the orientation, the cross-term is incorporated as

$$\mathbf{b}_k^i = \begin{bmatrix} \left(\mathbf{s}_k^{i,(0)} \right)^2 \\ \left(\mathbf{s}_k^{i,(1)} \right)^2 \\ \mathbf{s}_k^{i,(0)} \cdot \mathbf{s}_k^{i,(1)} \end{bmatrix}. \quad (13)$$

C. Axis Estimation

The predict step for the axis is carried out equivalently to (5), but using \mathbf{F}^1 and \mathbf{Q}^1 . For standard models as considered here, $\mathbf{F}^1 = \mathbf{I}^{2 \times 2}$, the two-by-two identity matrix. Non-zero values of \mathbf{Q}^1 can account for the object size changing over time.

The updated size estimate $\hat{\mathbf{l}}_{k|k}$ with covariance matrix $\mathbf{P}_{k|k}^1$ is computed using an improved semi-axis estimation procedure compared to the original MEM-EKF*, the derivation of which was presented in [15]. The closed-form Kalman filter update based on the quadratic pseudo-measurement of the original zero-centered measurement is carried out as [14], [15]

$$\hat{\mathbf{l}}_k^i = \hat{\mathbf{l}}_k^{i-1} + \mathbf{C}_{k,i}^{\mathbf{a},\mathbf{l}} \left(\mathbf{C}_{k,i}^{\mathbf{a},\mathbf{a}} \right)^{-1} \left(\mathbf{a}_k^i - \mathbb{E}(\mathbf{a}_k^i) \right), \quad (14a)$$

$$\mathbf{P}_k^{1,i} = \mathbf{P}_k^{1,i-1} - \mathbf{C}_{k,i}^{\mathbf{a},\mathbf{l}} \left(\mathbf{C}_{k,i}^{\mathbf{a},\mathbf{a}} \right)^{-1} \left(\mathbf{C}_{k,i}^{\mathbf{a},\mathbf{l}} \right)^T, \quad (14b)$$

using the expected pseudo-measurement

$$\mathbb{E}(\mathbf{a}_k^i) = \begin{bmatrix} \mathbf{W}_k^{\theta,(1,1)} + c \cdot \left(\mathbf{P}_k^{\hat{\mathbf{l}},i-1,(1,1)} + \left(\hat{\mathbf{l}}_k^{i-1,(1)} \right)^2 \right) \\ \mathbf{W}_k^{\theta,(2,2)} + c \cdot \left(\mathbf{P}_k^{\hat{\mathbf{l}},i-1,(2,2)} + \left(\hat{\mathbf{l}}_k^{i-1,(2)} \right)^2 \right) \end{bmatrix}, \quad (15)$$

and the pseudo-measurement covariance

$$\mathbf{C}_{k,i}^{\mathbf{a},\mathbf{a}} = \begin{bmatrix} 2 \cdot \left(\mathbb{E}(\mathbf{a}_k^i)^{(1)} \right)^2 & 2 \cdot \left(\mathbf{W}_k^{\theta,(1,2)} \right)^2 \\ 2 \cdot \left(\mathbf{W}_k^{\theta,(2,1)} \right)^2 & 2 \cdot \left(\mathbb{E}(\mathbf{a}_k^i)^{(2)} \right)^2 \end{bmatrix}, \quad (16)$$

where

$$\mathbf{W}_k^\theta = \text{rot} \left(-\hat{\theta}_k^{i-1} \right) \mathbf{W}_k \text{rot} \left(-\hat{\theta}_k^{i-1} \right)^T \quad (17)$$

is the axis-aligned version of the measurement covariance \mathbf{W}_k from (11).

The cross-covariance between \mathbf{a} and \mathbf{l} is given by $\mathbf{C}_{k,i}^{\mathbf{a},\mathbf{l}}$, which is a diagonal matrix with entries

$$\left(\mathbf{C}_{k,i}^{\mathbf{a},\mathbf{l}} \right)^{(0,0)} = 2 \cdot c \cdot \hat{\mathbf{l}}_k^{i-1,(1)} \cdot \mathbf{P}_k^{\hat{\mathbf{l}},i-1,(1,1)}, \quad (18a)$$

$$\left(\mathbf{C}_{k,i}^{\mathbf{a},\mathbf{l}} \right)^{(1,1)} = 2 \cdot c \cdot \hat{\mathbf{l}}_k^{i-1,(2)} \cdot \mathbf{P}_k^{\hat{\mathbf{l}},i-1,(2,2)}. \quad (18b)$$

D. Orientation Estimation

As before, the prediction of the orientation is a standard prediction step for the one-dimensional estimate, computing $\hat{\theta}_{k|k-1}$, $\mathbf{P}_{k|k-1}^\theta$.

To compute the updated orientation estimate $\hat{\theta}_{k|k}$ and its variance $\mathbf{P}_{k|k}^\theta$, we make use of (parts of) the results presented in [9], where the MEM-EKF* was originally described. The update is carried out analogously to Section C, but for the second pseudo-measurement \mathbf{b}_k^i and correspondingly different realizations for the expected pseudo-measurement and the two covariances. It reads

$$\hat{\theta}_k^i = \hat{\theta}_k^{i-1} + \mathbf{C}_{k,i}^{\mathbf{b},\theta} \left(\mathbf{C}_{k,i}^{\mathbf{b},\mathbf{b}} \right)^{-1} \left(\mathbf{b}_k^i - \mathbb{E}(\mathbf{b}_k^i) \right), \quad (19a)$$

$$\mathbf{P}_k^{\theta,i} = \mathbf{P}_k^{\theta,i-1} - \mathbf{C}_{k,i}^{\mathbf{b},\theta} \left(\mathbf{C}_{k,i}^{\mathbf{b},\mathbf{b}} \right)^{-1} \left(\mathbf{C}_{k,i}^{\mathbf{b},\theta} \right)^T. \quad (19b)$$

Computation of the three required expectations is slightly more involved, as the derivation requires linearization. For brevity, we will omit detailed explanations and refer to [9] for a comprehensive discussion and derivation.

The definition of the expectations makes use of

$$\mathbf{V} = \begin{bmatrix} 1 & 0 & 0 & 0 \\ 0 & 0 & 0 & 1 \\ 0 & 1 & 0 & 0 \end{bmatrix}, \quad \tilde{\mathbf{V}} = \begin{bmatrix} 1 & 0 & 0 & 0 \\ 0 & 0 & 0 & 1 \\ 0 & 0 & 1 & 0 \end{bmatrix}, \quad (20a)$$

$$\mathbf{C}_h = c \cdot \mathbf{I}^{2 \times 2}, \quad (20b)$$

$$\mathbf{S}_k^i = \text{rot} \left(\hat{\theta}_k^{i-1} \right) \hat{\mathbf{D}}_k^{i-1}, \quad (20c)$$

$$\mathbf{J}_{k,1}^i = \begin{bmatrix} -\hat{\mathbf{l}}_k^{i-1,(1)} \cdot \sin(\hat{\theta}_k^{i-1}) & -\hat{\mathbf{l}}_k^{i-1,(2)} \cdot \cos(\hat{\theta}_k^{i-1}) \end{bmatrix}^T, \quad (20d)$$

$$\mathbf{J}_{k,2}^i = \begin{bmatrix} \hat{\mathbf{l}}_k^{i-1,(1)} \cdot \cos(\hat{\theta}_k^{i-1}) & -\hat{\mathbf{l}}_k^{i-1,(2)} \cdot \sin(\hat{\theta}_k^{i-1}) \end{bmatrix}^T, \quad (20e)$$

with $\hat{\mathbf{D}}_k^{i-1}$ as given in (8b). Furthermore, \mathbf{S}_k^i is divided in its first and second row, in the following denoted by $\mathbf{S}_{k,1}^i$ and $\mathbf{S}_{k,2}^i$, respectively. Based on (20), we moreover define

$$\mathbf{C}_{k,\text{I}}^i = \mathbf{S}_k^i \mathbf{C}_h \left(\mathbf{S}_k^i \right)^T, \quad (21a)$$

$$\mathbf{C}_{k,\text{II}}^{i,(m,n)} = \text{tr} \left(\mathbf{P}_k^{\theta,i-1} \left(\mathbf{J}_{k,n}^i \right)^T \mathbf{C}_h \mathbf{J}_{k,m}^i \right), \quad m, n \in \{1, 2\}, \quad (21b)$$

$$\mathbf{C}_{k,\text{s}}^i = \mathbf{W}_k + \mathbf{C}_{k,\text{I}}^i + \mathbf{C}_{k,\text{II}}^i, \quad (21c)$$

$$\mathbf{M}_k^i = \begin{bmatrix} 2 \cdot \mathbf{S}_{k,1}^i \mathbf{C}_h \mathbf{J}_{k,1}^i \\ 2 \cdot \mathbf{S}_{k,2}^i \mathbf{C}_h \mathbf{J}_{k,2}^i \\ \mathbf{S}_{k,1}^i \mathbf{C}_h \mathbf{J}_{k,2}^i + \mathbf{S}_{k,2}^i \mathbf{C}_h \mathbf{J}_{k,1}^i \end{bmatrix}, \quad (21d)$$

Finally, the three desired expectations are given by

$$\mathbb{E}(\mathbf{b}_k^i) = \mathbf{V} \text{vect} \left(\mathbf{C}_{k,\text{s}}^i \right) \quad (22a)$$

$$\mathbf{C}_{k,i}^{\mathbf{b},\mathbf{b}} = \mathbf{V} \left(\mathbf{C}_{k,\text{s}}^i \otimes \mathbf{C}_{k,\text{s}}^i \right) \left(\mathbf{V} + \tilde{\mathbf{V}} \right)^T, \quad (22b)$$

$$\mathbf{C}_{k,i}^{\mathbf{b},\theta} = \mathbf{P}_k^{\theta,i-1} \mathbf{M}^i, \quad (22c)$$

where vect creates a column vector from a matrix by stacking its columns as defined in [9] and \otimes is the Kronecker product.

Algorithm 2: Batch-based MEM-QKF

- 1) **Predict:** Compute $\hat{\mathbf{m}}_k^0, \mathbf{P}_k^{\mathbf{m},0}, \hat{\mathbf{i}}_k^0, \mathbf{P}_k^{\mathbf{l},0}, \hat{\theta}_k^0, \mathbf{P}_k^{\theta,0}$ using three standard predict steps following (5) with the corresponding process noise covariances matrices for each component.
- 2) **Update:**
 - If only a single measurement is available, employ the update from Algorithm 1,
 - a) Compute the kinematic posterior $\hat{\mathbf{m}}_{k|k}, \mathbf{P}_{k|k}^{\mathbf{m}}$ using (24),
 - b) Compute the stacked axis pseudo-measurement $\tilde{\mathbf{a}}_k$ using (25),
 - c) Compute the axis posterior $\hat{\mathbf{i}}_{k|k}, \mathbf{P}_{k|k}^{\mathbf{l}}$ as defined in (26)
 - d) Compute the orientation pseudo-measurements using (33),
 - e) Compute the orientation posterior $\hat{\theta}_{k|k}, \mathbf{P}_{k|k}^{\theta}$ from (31).

V. BATCH-BASED FORMULATION

In the previous section, the proposed algorithm was introduced in a sequential manner, i.e., all measurements are explicitly iterated once in order to compute the overall posterior. This is significantly more efficient than algorithms that perform multiple passes over the set of measurements, such as the iterative Variational Bayes Random Matrix (VBRM) [13] or the sample-based MEM-RBPF [15]. Nevertheless, for practical applications, even better computational efficiency can be desirable. This can be achieved by performing the measurement update *batch-based*, i.e., performing a single update using all available measurements. One of the most prominent algorithms using this strategy is the highly efficient original RM algorithm [8]. A recent example is the MEM-EIF [19], which is a batch-based variant of the MEM-EKF*.

In the following sections, we will present the batch-based formulation of the proposed MEM-QKF. This variant follows the same approach as the previous section, decoupling the kinematics, orientation and semi-axis lengths. However, each of the three posteriors is computed using a single Kalman filter-based update making use of all measurements. Therefore, the iteration index i is omitted, and instead explicit notation of the posterior $(k|k)$ and prior $(k|k-1)$ is used.

For the case that a single measurement is available, the update from the previous section can readily be employed, avoiding the approximations needed for the derivation of the batch-based update. For $|\mathbf{Z}_k| > 1$, the batch-based algorithm is described in the following, and summarized in Algorithm 2.

A. Kinematic Batch Update

The batch-based update of the kinematics is straightforward. As done by, e.g., the RM [8] algorithm, it is

carried out using a pseudo-measurement $\bar{\mathbf{z}}_k \in \mathbb{R}^2$, which is given by the mean of the measurements

$$\bar{\mathbf{z}}_k = \frac{1}{M_k} \sum_{i=1}^{M_k} \mathbf{z}_k^i. \quad (23)$$

The update formula therefore is given by

$$\hat{\mathbf{m}}_{k|k} = \hat{\mathbf{m}}_{k|k-1} + \mathbf{K}_k (\bar{\mathbf{z}}_k - \mathbf{H}\hat{\mathbf{m}}_k^{i-1}), \quad (24a)$$

$$\mathbf{P}_{k|k}^{\mathbf{m}} = \mathbf{P}_{k|k-1}^{\mathbf{m}} - \mathbf{K}_k^i \mathbf{H} \mathbf{P}_{k|k-1}^{\mathbf{m}}, \quad (24b)$$

$$\mathbf{K}_k = \mathbf{P}_{k|k-1}^{\mathbf{m}} \mathbf{H}^T \left(\mathbf{H} \mathbf{P}_{k|k-1}^{\mathbf{m}} \mathbf{H}^T + \frac{1}{M_k} \tilde{\mathbf{R}}_k \right)^{-1}. \quad (24c)$$

As for the sequential update, $\tilde{\mathbf{R}}_k$ is given by (7). Implementations of non-linear or otherwise more complex kinematic models can directly use $\bar{\mathbf{z}}_k$ with corresponding covariance $\frac{1}{M_k} \tilde{\mathbf{R}}_k$.

B. Axis Batch Update

In order to compute the batch-based update of the semi-axis, a stacked version of the pseudo-measurements given in Section C is used. This stacked pseudo-measurement is defined as

$$\tilde{\mathbf{a}}_k = \begin{bmatrix} (\mathbf{s}_k^{0,(0)})^2 \\ (\mathbf{s}_k^{0,(1)})^2 \\ \vdots \\ (\mathbf{s}_k^{M_k,(0)})^2 \\ (\mathbf{s}_k^{M_k,(1)})^2 \end{bmatrix}, \quad (25)$$

with $\tilde{\mathbf{a}}_k \in \mathbb{R}^{2 \cdot M_k}$ i.e., all \mathbf{s}_k^i , which are computed following (9), are stacked into a single vector.

The update is then given by

$$\hat{\mathbf{i}}_{k|k} = \hat{\mathbf{i}}_k^0 + \mathbf{C}_k^{\tilde{\mathbf{a}},\mathbf{l}} \left(\mathbf{C}_k^{\tilde{\mathbf{a}},\tilde{\mathbf{a}}} \right)^{-1} (\tilde{\mathbf{a}}_k - \mathbb{E}(\tilde{\mathbf{a}}_k)), \quad (26a)$$

$$\mathbf{P}_{k|k}^{\mathbf{l}} = \mathbf{P}_{k|k-1}^{\mathbf{l}} - \mathbf{C}_k^{\tilde{\mathbf{a}},\mathbf{l}} \left(\mathbf{C}_k^{\tilde{\mathbf{a}},\tilde{\mathbf{a}}} \right)^{-1} \left(\mathbf{C}_k^{\tilde{\mathbf{a}},\mathbf{l}} \right)^T, \quad (26b)$$

where now the covariances based on $\tilde{\mathbf{a}}_k$ are required, rather than those based on \mathbf{a}_k^i as before. The cross-covariance $\mathbf{C}_k^{\tilde{\mathbf{a}},\mathbf{l}} \in \mathbb{R}^{2 \times (2 \cdot M_k)}$ between the stacked measurement and the semi-axis state is given by

$$\mathbf{C}_k^{\tilde{\mathbf{a}},\mathbf{l}} = \begin{bmatrix} \zeta_k^1 & 0 & \zeta_k^1 & 0 & \dots & \zeta_k^1 & 0 \\ 0 & \zeta_k^2 & 0 & \zeta_k^2 & \dots & 0 & \zeta_k^2 \end{bmatrix}, \quad (27a)$$

$$\zeta_k^1 = 2 \cdot c \cdot \hat{\mathbf{i}}_{k|k-1}^{(1)} \cdot \mathbf{P}_{k|k-1}^{\hat{\mathbf{i}},(1,1)}, \quad (27b)$$

$$\zeta_k^2 = 2 \cdot c \cdot \hat{\mathbf{i}}_{k|k-1}^{(2)} \cdot \mathbf{P}_{k|k-1}^{\hat{\mathbf{i}},(2,2)}. \quad (27c)$$

which follows from (18), where the values from the previous measurement iterations need to be replaced with the prior, i.e., the predicted axis state consisting of $\hat{\mathbf{i}}_{k|k-1}$ and $\mathbf{P}_{k|k-1}^{\mathbf{l}}$.

Approximating the pseudo-measurements as independent, the covariance of the stacked pseudo-measurement

$\mathbf{C}_k^{\tilde{\mathbf{a}}, \tilde{\mathbf{a}}} \in \mathbb{R}^{(2 \cdot M_k) \times (2 \cdot M_k)}$ is given by a block diagonal matrix of the individual pseudo-measurement covariances:

$$\mathbf{C}_k^{\tilde{\mathbf{a}}, \tilde{\mathbf{a}}} = \text{blkdiag} \left(\mathbf{C}_{k,0}^{\mathbf{a}, \mathbf{a}}, \dots, \mathbf{C}_{k,M_k}^{\mathbf{a}, \mathbf{a}} \right) , \quad (28)$$

where it is important to note that, as for the cross-covariance, each of the $\mathbf{C}_{k,i}^{\mathbf{a}, \mathbf{a}}$ as defined in (16) needs to be computed from the prediction instead of the previous iteration.

A naive implementation would require inversion of a $(2 \cdot M_k) \times (2 \cdot M_k)$ -dimensional matrix for the batch-update, which can cause numerical instability and is generally computationally inefficient. However, when computing $\mathbf{C}_{k,i}^{\mathbf{a}, \mathbf{a}}$ from the predicted estimate, each of the individual pseudo-measurements will have identical estimated covariances, since (16) only depends on $\mathbb{E}(\tilde{\mathbf{a}}_k^i)$ given in (15), which in turn depends only on the prior estimate. Therefore, instead of first computing a large block diagonal matrix and then inverting it, one can directly make use of

$$\left(\mathbf{C}_k^{\tilde{\mathbf{a}}, \tilde{\mathbf{a}}} \right)^{-1} = \text{blkdiag} \left(\left(\mathbf{C}_k^{\tilde{\mathbf{a}}, \tilde{\mathbf{a}}} \right)^{-1}, \dots, \left(\mathbf{C}_k^{\tilde{\mathbf{a}}, \tilde{\mathbf{a}}} \right)^{-1} \right) , \quad (29)$$

where $\mathbf{C}_k^{\tilde{\mathbf{a}}, \tilde{\mathbf{a}}}$ is readily computed from (15) and (16) using the predicted axis state. By this means, merely a single 2×2 matrix needs to be inverted, which is then stacked into a larger block diagonal for $\left(\mathbf{C}_k^{\tilde{\mathbf{a}}, \tilde{\mathbf{a}}} \right)^{-1}$.

Finally, the expectation of the stacked pseudo-measurement follows the same principle as the stacked pseudo-measurement (25), and is computed analogously to (15), i.e., $\mathbb{E}(\tilde{\mathbf{a}}_k^i) \in \mathbb{R}^{2 \cdot M_k}$ and

$$\mathbb{E}(\tilde{\mathbf{a}}_k^i) = [\rho_k^1 \ \rho_k^2 \ \rho_k^1 \ \rho_k^2 \ \dots \ \rho_k^1 \ \rho_k^2]^T , \quad (30a)$$

$$\rho_k^1 = \mathbf{W}_k^{\theta, (1,1)} + c \cdot \left(\mathbf{P}_{k|k-1}^{\hat{\mathbf{l}}, (1,1)} + \left(\hat{\mathbf{l}}_{k|k-1}^{(1)} \right)^2 \right) , \quad (30b)$$

$$\rho_k^2 = \mathbf{W}_k^{\theta, (2,2)} + c \cdot \left(\mathbf{P}_{k|k-1}^{\hat{\mathbf{l}}, (2,2)} + \left(\hat{\mathbf{l}}_{k|k-1}^{(2)} \right)^2 \right) . \quad (30c)$$

C. Orientation Batch Update

Finally, for the orientation, in previous related work [19] a closed-form batch update of the orientation has already been derived based on the information form of the update. For the derivation, we refer to [19], and here only present the resulting formulas when applied for the proposed algorithm.

A key difference is that [19] made use of the kinematic posterior for the shape update. To avoid double counting of measurement information, we instead make use of $\bar{\mathbf{z}}_k$, i.e., the mean of measurements instead, which is consistent with the computation of pseudo-measurements above in (13). We make use of the same helper variables already defined in the sequential orientation update, i.e., (20) and (21) are again used in the following.

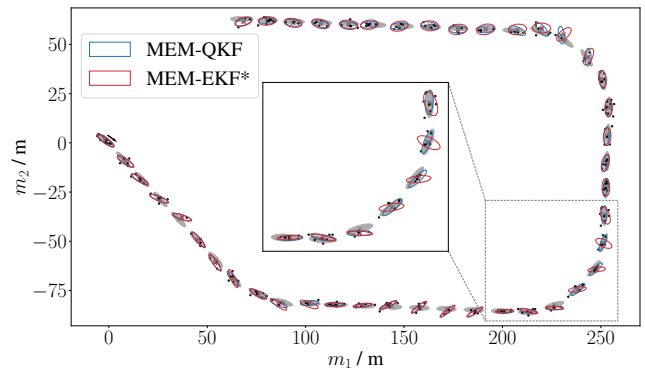


Fig. 2: Example qualitative results for tracking a maneuvering elliptical object with the proposed MEM-QKF and the MEM-EKF* [9] on the simulated trajectory.

The posterior orientation estimate and its variance are computed as

$$\hat{\theta}_{k|k} = \mathbf{P}_{k|k}^{\theta} \xi_{k|k}^{\theta} , \quad (31a)$$

$$\mathbf{P}_{k|k}^{\theta} = \left(\left(\mathbf{P}_{k|k-1}^{\theta} \right)^{-1} + |\mathbf{Z}_k| \cdot \mathbf{M}_k^T \left(\mathbf{P}_k^t \right)^{-1} \mathbf{M}_k \right)^{-1} , \quad (31b)$$

where

$$\mathbf{P}_k^t = \mathbf{C}_k^{\mathbf{b}, \mathbf{b}} - \mathbf{M}_k \mathbf{P}_{k|k-1}^{\theta} , \quad (32a)$$

$$\xi_{k|k}^{\theta} = \xi_{k|k-1}^{\theta} + \mathbf{M}_k^T \left(\mathbf{P}_k^t \right)^{-1} \Xi_k , \quad (32b)$$

$$\Xi_k = \sum_{i=1}^{|\mathbf{Z}_k|} \mathbf{b}^i - \mathbb{E}(\mathbf{b}_k) + \mathbf{M}_k \cdot \hat{\theta}_{k|k-1} , \quad (32c)$$

$$\xi_{k|k-1}^{\theta} = \left(\mathbf{P}_{k|k-1}^{\theta} \right)^{-1} \cdot \hat{\theta}_{k|k-1} . \quad (32d)$$

Analogously to (13), the pseudo-measurements can be computed using Kronecker notation as

$$\mathbf{b}^i = \mathbf{V} (\mathbf{s}_k^i \otimes \mathbf{s}_k^i) \quad (33)$$

and the expected pseudo-measurement equivalently to the sequential update, i.e., as defined in (22a). The pseudo-measurement covariance, $\mathbf{C}_k^{\mathbf{b}, \mathbf{b}}$ is computed as in (22b), since the individual pseudo-measurements are identical.

VI. SIMULATION STUDY

To confirm the effectiveness of the proposed method, named MEM-QKF, under the given assumptions, an extensive simulation study was carried out. Two scenarios were assessed: Firstly, a standard simulation based on a target following a pre-defined trajectory (with added zero-mean process noise) as shown in Fig. 2, where measurement parameters were varied to evaluate the trackers' robustness. Secondly, a stationary setting in which only a single measurement was received in each step, requiring sequential processing of the data.

Multiple existing methods have been chosen as reference algorithms: The MEM-EKF* [9], which is a closed-form algorithm that can be seen as the predecessor of the

TABLE I: Mean error squared GWD for all trackers on 500 Monte Carlo runs of each of the three scenarios. Batch-based methods are separated in their own section.

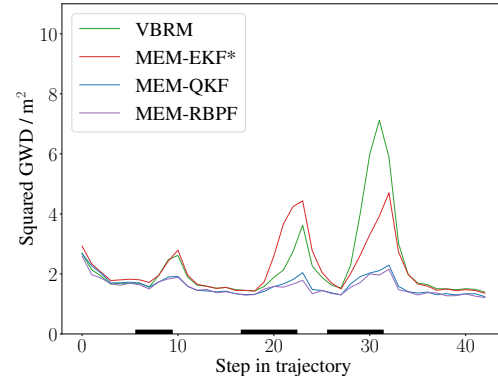
Method	Moderate	Noisy	Sparse
MEM-EKF* [9]	2.185 m ²	2.974 m ²	4.738 m ²
VBRM [13]	2.242 m ²	3.529 m ²	4.143 m ²
MEM-RBPF [15]	1.569 m ²	2.089 m ²	3.284 m ²
MEM-QKF (ours)	1.626 m ²	2.158 m ²	3.380 m ²
RM [8]	3.494 m ²	4.377 m ²	10.194 m ²
MEM-EIF [19]	2.387 m ²	3.014 m ²	4.802 m ²
Batch MEM-QKF (ours)	2.114 m ²	2.755 m ²	4.188 m ²

proposed filter. Furthermore, the closely related MEM-RBPF [15], which is a sampling-based filter from the family of MEM algorithms. Additionally, the VBRM [13] has been selected as its explicit focus on orientation estimation makes it a good match for the evaluation.

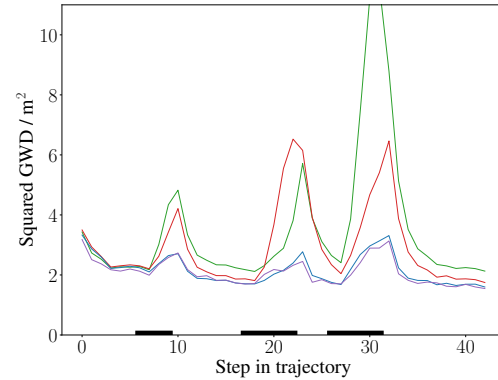
Of course, the batch-based variant needs to be compared with other batch-based trackers. Here, the RM tracker [8] has been employed as a baseline algorithm. Furthermore, the MEM-EIF [19] is a recent state-of-the-art batch-based tracker closely related to the MEM-EKF*.

To assess the quality of the tracking results jointly for the position and shape estimates, the Gaussian Wasserstein Distance (GWD) [33] was used, as originally suggested by [34]. The methods' parameters were chosen according to the parameters of the simulation. The number of iterations l_{max} for VBRM was set to 10, as suggested in the original work [13]. The parameter γ , which controls the rate of change of the shape, was set to $\gamma = 0.98$. For the RM tracker, the scalar certainty was decayed by $\exp(-\frac{1}{1.6})$ for the moving object, and by $\exp(-\frac{1}{10})$ for the stationary one. These values were tuned to yield accurate tracking results and avoid divergence of the tracking results. The number of particles for the MEM-RBPF was 50 as suggested in the original article [15]. As suggested in [19, Section IV-A], for the MEM-based methods, we add a parameter ψ to threshold the variance of the semi-axis to avoid the Gaussian distribution from reaching into negative values. The variance of the semi-axis are cut off at $(\psi \cdot \mathbf{I})^2$. This value was selected as 0.4 for the MEM-EKF*, as suggested in [19]. For the MEM-EIF, it was chosen even lower as 0.15, leading to improved results in our experiments. For our own algorithm, we employed this threshold only for the batch-based variant, setting the parameter to 0.4 for the simulation.

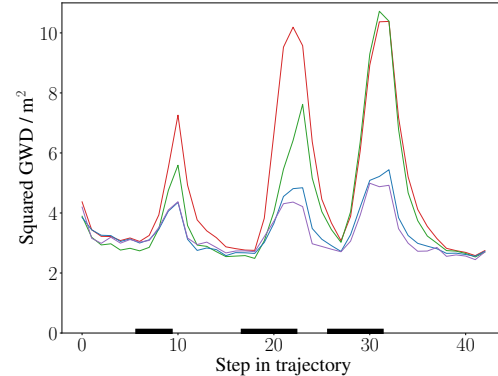
For all experiments, the expected value of the prior of the state was passed to the tracker along with the corresponding covariance. The ground truth was sampled from this distribution, without the result being known to the tracker. An implementation of the method as well as the presented experiments including the real-world radar data is available online².



(a) Moderate measurement data.



(b) Noisy measurement data.



(c) Sparse measurement data.

Fig. 3: Results of the evaluation for three different measurement settings, each averaged over 500 Monte Carlo runs. Black bars indicate time steps during which the object turned.

A. Moving Target

In the first set of experiments, the object followed the path shown in Fig. 2, modeled to follow the evaluation trajectory used in [9]. The shape prior had expected value 5 m and 2 m for the semi-axis, with covariance $\mathbf{I}_{2 \times 2}$. The kinematic prior covariance matrix was $\text{diag}(2, 2, 0.5, 0.5)$. The process noise for the kinematics was 1 for the position and 2 for the velocity. The target orientation was aligned with the velocity, which was encoded with variance 0.1 radians in all trackers. The object performs three turns, violating the employed constant velocity

²<https://github.com/Fusion-Goettingen/>

TABLE II: Mean orientation estimation error throughout 500 Monte Carlo runs of the moderate measurement setting. Batch-based methods are separated in their own section.

Method	Orientation Error (rad)
MEM-EKF* [9]	0.267
VBRM [13]	0.248
MEM-RBPF [15]	0.190
MEM-QKF (ours)	0.205
RM [8]	0.299
MEM-EIF [19]	0.219
Batch MEM-QKF (ours)	0.225

motion model. Employing a more complex, non-linear model could improve tracking performance, however, it is of great interest to evaluate how the trackers perform when the motion model is temporarily violated. This is because a key challenge of EOT is dealing with the fact that measurement locations can shift due to either kinematic or shape changes of the object.

A total of 500 Monte Carlo runs were performed for three settings. These settings differ in two parameters, the expected number of measurements λ and the measurement noise covariance matrix \mathbf{R} . The realizations of these values were as follows:

- Moderate: $\lambda = 12$, $\mathbf{R} = \text{rot}(\frac{\pi}{4}) \text{diag}(\frac{3}{2}, \frac{2}{3}) \text{rot}(\frac{\pi}{4})^T$
- Noisy: $\lambda = 12$, $\mathbf{R} = \text{rot}(\frac{\pi}{4}) \text{diag}(3, 1) \text{rot}(\frac{\pi}{4})^T$
- Sparse: $\lambda = 6$, $\mathbf{R} = \text{rot}(\frac{\pi}{4}) \text{diag}(\frac{3}{2}, \frac{2}{3}) \text{rot}(\frac{\pi}{4})^T$

Anisotropic covariance matrices are used to simulate sensors of interest for EOT, e.g., radar. The number of measurements in each step was drawn from a Poisson distribution with mean λ .

The mean tracking error over time of the methods measured in GWD is shown in Fig. 3. Additionally, the overall averages across all runs of each of the settings are summarized in Table I. As mentioned above, situations in which the motion of the target is not accurately predicted cause significant increase in error. This effect is aggravated in the sparse and noisy settings. Here, the effective difference between methods is best visible. The sampling-based MEM-RBPF consistently performs best throughout all settings. The closed-form RM algorithm is affected most, whereas the optimization-based VBRM can recover noticeably faster. Our proposed method exhibits robust behavior, almost matching the performance of the sampling-based RBPF. This leads to a significant reduction in error compared to the MEM-EKF*. This can also be seen in the qualitative results presented in Fig. 2. The summary presented in Table I confirms the observations visible in Fig. 3: In all settings, the mean error of the MEM-RBPF is lowest, closely followed by the proposed method. A noticeable gap between the error of these two methods and all other reference methods, including the optimization-based VBRM, can be observed.

Beyond the comparison in GWD, we compare the orientation estimation quality in Table II. Generally, the orientation error and the GWD clearly correlate as expected. The RBPF, which has particular emphasis on the

TABLE III: Mean runtime of the compared methods across the 500 Monte Carlo runs in the moderate measurement setting. For the VBRM method, the number of variational Bayes iterations was 10, and the number of particles for the MEM-RBPF was 50, as suggested in the original articles. Batch-based methods are separated in their own section.

Method	Mean Runtime
MEM-EKF* [9]	5.375 ms
VBRM [13]	9.560 ms
MEM-RBPF [15]	9.534 ms
MEM-QKF (ours)	5.027 ms
RM [8]	1.067 ms
MEM-EIF [19]	1.743 ms
Batch MEM-QKF (ours)	1.597 ms

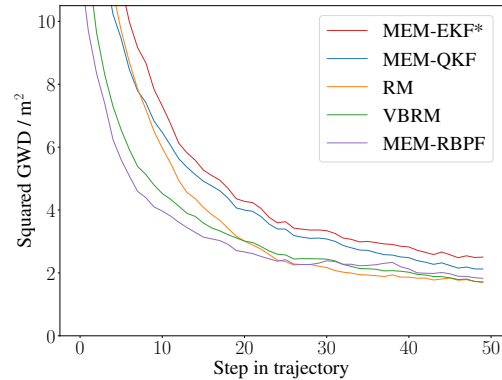


Fig. 4: Estimation error in GWD for a stationary target with a single measurement per step, averaged over 500 Monte Carlo runs.

orientation estimation in its design, performs best. Noticeably, the proposed MEM-QKF performs decidedly better than the MEM-EKF*, despite the mathematical similarity in their respective orientation estimation procedures. We attribute this to two factors: First, the improved semi-axis estimation procedures allow for better orientation estimation. Second, the fact that by approximating the correlations between orientation and axis as zero, fewer errors are introduced.

The runtime of the methods is compared in Table III, and also below in Fig. 6. All methods were implemented in python and run on the same system using an Intel i5-12600K processor. The runtime was measured during the Monte Carlo runs of the moderate measurement setting. The results of this confirm that the proposed closed-form method is significantly faster than the optimization-based VBRM and the sampling-based MEM-RBPF. Note that the run times of these methods vary depending on the choice of the number of iterations and particles, respectively. Compared to the MEM-EKF*, which also is computed in closed-form, the difference is smaller, yet still visible. We attribute the runtime difference between these two methods to the fact that the MEM-EKF* requires larger matrices in the filtering equations, meaning the computation of, e.g., matrix inverses is more expensive. Overall, the batch-based RM approach is nevertheless even more computationally efficient, outperforming all other methods.

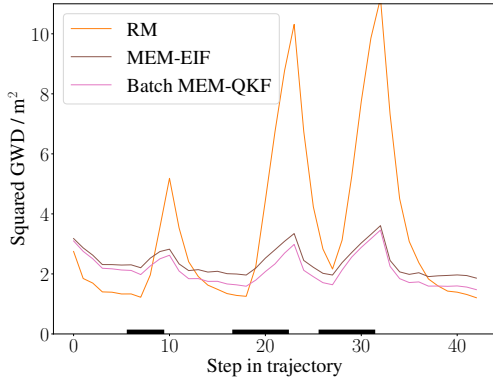


Fig. 5: Results of the three batch-based algorithms in the moderate measurement setting, averaged over 500 Monte Carlo runs. Black bars indicate time steps during which the object turned.

B. Single Measurement per Step

As a second simulation study, we evaluated the results of the methods for the setting of a stationary target with expected size 8×4 meters emitting exactly one measurement per time step. The measurement noise was $\mathbf{R} = \mathbf{I}_{2 \times 2}$. Results are visualized in Fig. 4. All trackers were initialized with variance of 0.1 for the position, but the initial orientation uncertainty was π and the initial covariance of the axis lengths $\text{diag}(4, 2)$. This means the kinematics were more or less entirely known to the trackers, but due to the strong noise on the shape prior, the convergence behavior of the extent estimation of each method can be studied. As for a single measurement, the batch approximations for the proposed algorithm and the MEM-EKF* are not needed, these are not included in the plot. Furthermore, it is important to note that for the RM approach to converge at all, the decay of the scalar certainty parameter of the inverse Wishart distribution modeling the shape needs to be vastly reduced compared to the previous experiment.

With this in mind, the RM approach converges to the lowest error of all methods, albeit after a slower convergence phase than the VBRM and MEM-RBPF. These two methods converge to a similarly low error, with the MEM-RBPF converging the fastest, likely due to the fact that it simultaneously evaluates multiple hypotheses about the orientation. The MEM-EKF* and MEM-QKF converge to slightly higher overall error. As in the previous experiment, the MEM-QKF outperforms the MEM-EKF*, both in final error and throughout the convergence phase. This experiment demonstrated that (10) is a suitable approach for dealing with a stream of measurements.

C. Batch-based Variant

The batch-based variant proposed in Section V has been analyzed using similar experiments as described above. Tables I, II, and III include separate sections containing aggregated mean results for the three batch-based algorithms. Furthermore, the mean error over 500

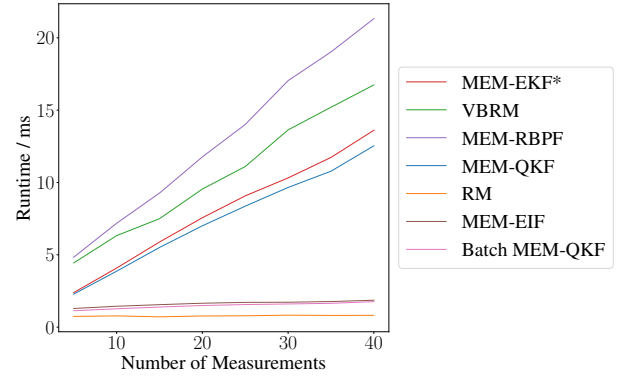


Fig. 6: Runtime of the evaluated methods for different number of processed measurements, averaged over 50 Monte Carlo runs of different settings with increasing measurement count.

Monte Carlo runs of the moderate measurement setting for the batch-based methods is presented in Fig. 5.

Initially, the RM algorithm performs best, however, it is severely affected by the turns, leading to very large spikes in error. These are significantly less pronounced for the two MEM-based algorithms. Out of these two, our proposed method consistently produces more accurate results compared to the MEM-EIF.

Finally, Fig. 6 presents an analysis of the runtime of the evaluated methods over the number of measurements. For this experiment, the same settings as in the moderate measurement settings have been used. However, the number of measurements in each time step was varied between runs, and in each step fixed to the respective number, rather than drawn from a Poisson distribution as before. The efficiency improvement of the proposed batch-based variant can be clearly seen in this figure. While it does not quite match the computational efficiency of the RM approach, it significantly outperforms all algorithm processing measurements sequentially. The similar MEM-EIF [19] yields almost identical runtime.

In summary, the batch-based variant of the proposed MEM-QKF yields a tracker of high computational efficiency. Still, the tracking results are of high quality, leading to the fact that the tracker nevertheless outperforms state-of-the-art sequential algorithms, as seen in Table I.

VII. REAL-WORLD EVALUATION

In order to assess the applicability of the discussed tracking algorithms to real-world data, we made use of radar data from the nuScenes [17] data set, an illustration of which is given in Fig. 7. nuScenes contains data from the automotive domain. For each object, consistent annotations throughout each scene are provided as oriented bounding boxes.



Fig. 7: Example image from the front camera in the nuScenes [17] data set, with radar data added as a scatter plot on top. Brighter colors indicate radar points in greater distance. Note the distributed radar detections across the vehicle turning left in front of the recording car.

A. Data Set

We extracted a set of 468 suitable trajectories of individual objects from the nuScenes data set, projected into Bird’s Eye View (BEV). For each object, radar measurements in its vicinity, defined by inflating the ground-truth annotation bounding box by 33%, were extracted in each time step. Only sequences belonging to one of the *vehicle* subclasses were extracted. The sequences were selected so that each consists of at least ten consecutive annotated time steps. Furthermore, only sequences with an average of at least four measurements per time step were included. We found that a threshold lower than that vastly reduced the overall performance, regardless of the employed tracker, indicating that the data quality in even sparser sequences was too low to yield reasonable tracking results. Some further insight into the distribution of the average number of measurements per step can be found below in Fig. 8.

The methods’ parameters were tuned to the data in a unified manner for all trackers where possible. Some methods require unique parameters, e.g., the number of iterations for VBRM. These were tuned individually to yield accurate tracking results on the data set. The initial covariance matrix for the kinematics was set to $\text{diag}(0.75, 0.75, 1, 1)$, and the kinematic process noise covariance to $\text{diag}(0.01, 0.01, 0.15, 0.15)$. For the orientation, the initial standard deviation was 10° and the process noise variance 0.01 radians. The variances for the major and minor semi-axes were 1.0 and 0.05, respectively, and their process noise variance 10^{-4} . The measurement noise was tuned to $\mathbf{I}_{2 \times 2} \cdot 0.01$. This rather small value stems from the fact that most measurements were indeed observed on the target surface. For VBRM, the parameter α was set to 6. For RM, the initial value for the certainty of the shape estimate was 20, and the decay of this during the predict step set to a factor of $\exp(-\frac{1}{5})$. The previously discussed threshold parameter ψ for the axis variance was set to 0.4 for the MEM-EKF*, and 0.15 for the batch-based variant of our own tracker as well as the MEM-EIF.

TABLE IV: Comparison of all reference methods with the proposed approach on 468 real-world automotive radar sequences. The median and the mean GWS error of each method are shown. Methods are sorted by their mean error.

Method	Median GWS	Mean GWS
MEM-RBPF [15]	0.209	0.264
MEM-QKF (ours)	0.202	0.266
MEM-EKF* [9]	0.218	0.271
Batch MEM-QKF (ours)	0.216	0.275
VBRM [13]	0.229	0.282
RM [8]	0.234	0.293
MEM-EIF [19]	0.279	n/a

The prior for all trackers was chosen in the same way: For the kinematics, the mean of the measurements observed in the first time step was used. The velocity vector was set to $[0 \ 0]^T$. Eigenvalue decomposition of the sample covariance matrix of the first received measurements was used to acquire an initial orientation estimate. As this can be erroneous for sparse measurements, the corresponding uncertainty needs to be selected large enough. Finally, for the axis, the mean of all objects in the data set was used as a default value, yielding $[3.93, 1.26]^T$ for the semi-axis.

A rectangle is a more accurate description of the target shape than an ellipse. Following the underlying assumption that measurement sources are uniformly distributed on the entire object surface, the scaling factor is chosen as $c = \frac{1}{3}$ [31], which moment-matches a uniform distribution on a rectangle. Experimental results indeed confirmed that the tracking accuracy of all trackers was noticeably improved by adapting the scaling factor in this manner.

B. Evaluation

In theory, the GWD, used as the evaluation metric in Section VI, could be employed as the evaluation metric for the nuScenes data, as objects are represented by the very same parameters regardless of whether they represent rectangles or ellipses. However, the GWD is based on the object size. Hence, larger objects produce larger errors. Averaging across a data set with heterogeneous object sizes will then implicitly put more weight on correct estimates of larger objects, skewing the results.

In [35], these issues were discussed in greater detail, and it was suggested to normalize the GWD based on the ground truth object size, leading to the so-called Gaussian Wasserstein Score (GWS). Even though it is not a true metric, it maintains the desirable attributes of the GWD, while eliminating the bias towards large objects when evaluating on the data set at hand. In the following, the evaluation results for the nuScenes data will be presented in GWS.

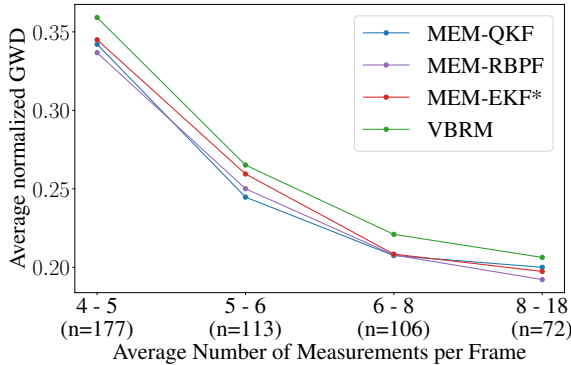


Fig. 8: Mean error in GWS of each method over the averaged number of measurements in the real-world radar sequences, grouped in four bins of similar size. Methods that are computed in closed-form are represented with solid lines, others with dashed ones.

C. Results

Compared to the stark difference in performance induced by the maneuvers simulated in Section VI, the performance of all evaluated trackers on the nuScenes data is rather close. This confirms that all trackers are indeed suitable approaches for radar-based target tracking.

Nevertheless, when evaluated across hundreds of trajectories, differences in estimation quality are visible. In Table IV, a comparison of each of the reference trackers with the proposed method is presented based on their mean and median GWS errors. Due to individual sequences on which no tracker performs well, the mean errors are generally noticeably higher than the median errors. The MEM-EKF yields generally unstable results on this data. It diverges on individual sequences, which causes the mean error to be unreasonably high. The proposed tracker yields the lowest median error and is only barely outperformed by the MEM-RBPF in mean error. Even the efficient batch-based variant outperforms several of the reference methods.

To evaluate the impact that the number of measurements has on the tracking accuracy, we grouped the extracted sequences based on their average number of measurements. To this end, we created bins of roughly equal number of trajectories for different values of mean number of measurements. The results are shown in Fig. 8. We focus on the tracking algorithms processing measurements sequentially, and leave out the three batch-based ones. Results for these are still included in Table IV for completeness.

In general, the VBRM yields slightly worse results than the MEM-based algorithms across all bins. The MEM-QKF and MEM-RBPF perform similarly, with the MEM-EKF* producing somewhat worse results than both in most bins.

Fig. 1 presents a qualitative example of tracking results on the nuScenes data set, comparing results of the MEM-EKF* and MEM-QKF. While similarity in

behavior is apparent, it can be seen that the proposed method converges faster, yielding overall better results.

VIII. CONCLUSION

In this article, we proposed an elliptical extended object tracker based on the idea of decoupling the kinematics, orientation, and axes estimation. This results in a deterministic, closed-form algorithm based on Kalman filter equations. Decoupling these three components has been shown to improve the individual estimation performance. For example, despite mathematical similarities, our tracker more accurately captures the orientation compared to existing closed-form solutions.

We furthermore proposed a highly efficient batch-based variant of the filter, requiring significantly less computational load. Nevertheless, this batch-based variant yields competitive results, even outperforming state-of-the-art algorithms that sequentially process all measurements one-by-one.

The results of the method demonstrate a significant advance in estimation accuracy. Our filter achieves comparable results to the best sampling-based reference method, outperforming closed-form and even optimization-based methods. This was demonstrated on hundreds of sequences of real-world radar data from the automotive domain, and further supported by a comprehensive simulation study where varying measurement conditions were tested.

For future work, integration into a multi-object tracker could be of interest. Furthermore, results on the radar data can be further improved by several means. Improved accounting for specifics of the measurement noise could be achieved by employing, e.g., an Unscented Kalman Filter (UKF) [36]. Improved motion models, e.g., via incorporation of an Interacting Multiple Model (IMM) [37], can also be studied. Here, the proposed method has clear advantages over many existing EOT algorithms due to the modularity arising from the decoupled approach. Replacing the kinematic estimator with existing non-linear complex motion models is straightforward, and no further derivations are necessary.

REFERENCES

- [1] K. Granström and M. Baum, “A tutorial on multiple extended object tracking,” in *TechRxiv*, Feb 2022.
- [2] M. Wieneke and W. Koch, “A PMHT approach for extended objects and object groups,” *IEEE Transactions on Aerospace and Electronic Systems*, vol. 48, no. 3, pp. 2349–2370, 2012.
- [3] K. Granström, M. Fatemi, and L. Svensson, “Gamma Gaussian inverse-Wishart Poisson multi-Bernoulli filter for extended target tracking,” in *2016 19th International Conference on Information Fusion (FUSION)*. IEEE, 2016, pp. 893–900.
- [4] S. Yang, L. M. Wolf, and M. Baum, “Marginal association probabilities for multiple extended objects without enumeration of measurement partitions,” in *2020 IEEE 23rd International Conference on Information Fusion (FUSION)*. IEEE, 2020, pp. 1–8.

[5] M. Baum and U. D. Hanebeck, "Extended object tracking with random hypersurface models," *IEEE Transactions on Aerospace and Electronic Systems*, vol. 50, no. 1, pp. 149–159, 2014.

[6] N. Wahlström and E. Özkan, "Extended target tracking using Gaussian processes," *IEEE Transactions on Signal Processing*, vol. 63, no. 16, pp. 4165–4178, 2015.

[7] M. Kumru and E. Özkan, "Tracking arbitrarily shaped extended objects using Gaussian processes," in *2024 27th International Conference on Information Fusion (FUSION)*. IEEE, 2024, pp. 1–8.

[8] M. Feldmann, D. Fränken, and W. Koch, "Tracking of extended objects and group targets using random matrices," *IEEE Transactions on Signal Processing*, vol. 59, no. 4, pp. 1409–1420, 2011.

[9] S. Yang and M. Baum, "Tracking the orientation and axes lengths of an elliptical extended object," *IEEE Transactions on Signal Processing*, vol. 67, no. 18, pp. 4720–4729, 2019.

[10] F. Govaers, "On independent axes estimation for extended target tracking," in *2019 Sensor Data Fusion: Trends, Solutions, Applications (SDF)*, 2019, pp. 1–6.

[11] M. Tesori, G. Battistelli, L. Chisci, and A. Farina, "L:OMEM-a fast filter to track maneuvering extended objects," in *2023 26th International Conference on Information Fusion (FUSION)*. IEEE, 2023, pp. 1–8.

[12] J. W. Koch, "Bayesian approach to extended object and cluster tracking using random matrices," *IEEE Transactions on Aerospace and Electronic Systems*, vol. 44, no. 3, pp. 1042–1059, 2008.

[13] B. Tuncer and E. Özkan, "Random matrix based extended target tracking with orientation: A new model and inference," *IEEE Transactions on Signal Processing*, vol. 69, pp. 1910–1923, 2021.

[14] M. Baum, F. Faion, and U. D. Hanebeck, "Modeling the target extent with multiplicative noise," in *2012 15th International Conference on Information Fusion*. IEEE, 2012, pp. 2406–2412.

[15] S. Steuernagel and M. Baum, "Extended object tracking by Rao-Blackwellized particle filtering for orientation estimation," *IEEE Transactions on Signal Processing*, vol. 73, pp. 2590–2602, 2025.

[16] Z. Zhao, H. Chen, and W. Zhang, "Adaptive elliptical extended object tracking based on deep reinforcement learning," *Measurement Science and Technology*, vol. 36, no. 5, 2025.

[17] H. Caesar, V. Bankiti, A. H. Lang, S. Vora, V. E. Liong, Q. Xu, A. Krishnan, Y. Pan, G. Baldan, and O. Beijbom, "nuScenes: A multimodal dataset for autonomous driving," in *Proceedings of the IEEE/CVF Conference on Computer Vision and Pattern Recognition*, 2020, pp. 11621–11631.

[18] S. Steuernagel and M. Baum, "Decoupled quadratic filter for extended object tracking using multiplicative noise," in *2025 Sensor Data Fusion: Trends, Solutions, Applications (SDF)*. IEEE, 2025, pp. 1–6.

[19] C. Gramsch, S. Yang, and H. Alqaderi, "A batch update using multiplicative noise modelling for extended object tracking," in *2024 27th International Conference on Information Fusion (FUSION)*. IEEE, 2024, pp. 1–8.

[20] J. Lan and X. R. Li, "Tracking of extended object or target group using random matrix: New model and approach," *IEEE Transactions on Aerospace and Electronic Systems*, vol. 52, no. 6, pp. 2973–2989, 2017.

[21] J. Lan, "Extended object tracking using random matrix with extension-dependent measurement numbers," *IEEE Transactions on Aerospace and Electronic Systems*, vol. 59, no. 4, pp. 4464–4477, 2023.

[22] S. Pei, Z. Wang, R. Li, J. Liu, P. Li, C. Chen, and W. Chen, "Constrained extended target tracking with random matrix and approximate projection," *IEEE Sensors Journal*, 2025.

[23] L. Zhang and J. Lan, "Extended object tracking using aspect ratio," *IEEE Transactions on Signal Processing*, 2024.

[24] S. Wang, C. Men, R. Li, T.-S. Yeo, and P. He, "Extended target tracking algorithm based on variational Bayes and axis estimation theory," *IEEE Transactions on Instrumentation and Measurement*, vol. 74, 2025, Art. no. 8507216.

[25] J. Zhang, C. Hu, R. Wang, Q. Jiang, M. Shi, L. Xu, and W. Tian, "An adaptive multivariate approach to dynamic group target tracking using variational inference," *IEEE Transactions on Aerospace and Electronic Systems*, 2025.

[26] K. K. Şahin, A. E. Balcı, and E. Özkan, "Random matrix extended target tracking for trajectory-aligned and drifting targets," *IET Radar, Sonar & Navigation*, vol. 18, no. 11, pp. 2247–2263, 2024.

[27] Z. Wen, J. Lan, L. Zheng, and T. Zeng, "Velocity-dependent orientation estimation using variance adaptation for extended object tracking," *IEEE Signal Processing Letters*, 2024.

[28] Z. Wen, L. Zheng, and T. Zeng, "Extended object tracking using an orientation vector based on constrained filtering," *Remote Sensing*, vol. 17, no. 8, p. 1419, 2025.

[29] M. Li, J. Lan, and X. R. Li, "Tracking of elliptical object with unknown but fixed lengths of axes," *IEEE Transactions on Aerospace and Electronic Systems*, vol. 59, no. 5, pp. 6518–6533, 2023.

[30] X. Zheng, Y. Zhang, S. Wu, and H. Li, "Extended object tracking with inaccurate heavy-tailed noises," *IEEE Transactions on Instrumentation and Measurement*, 2025.

[31] S. Steuernagel, K. Thormann, and M. Baum, "Random matrix-based tracking of rectangular extended objects with contour measurements," in *2024 27th International Conference on Information Fusion (FUSION)*. IEEE, 2024, pp. 1–8.

[32] M. Feldmann and W. Koch, "Comments on "Bayesian approach to extended object and cluster tracking using random matrices"," *IEEE Transactions on Aerospace and Electronic Systems*, vol. 48, no. 2, pp. 1687–1693, 2012.

[33] C. R. Givens and R. M. Shortt, "A class of Wasserstein metrics for probability distributions," *The Michigan Mathematical Journal*, vol. 31, no. 2, pp. 231–240, 1984.

[34] S. Yang, M. Baum, and K. Granström, "Metrics for performance evaluation of elliptic extended object tracking methods," in *2016 IEEE International Conference on Multisensor Fusion and Integration for Intelligent Systems (MFI)*. IEEE, 2016, pp. 523–528.

[35] S. Steuernagel, K. Thormann, and M. Baum, "Evaluation scores for elliptic extended object tracking considering diverse object sizes," in *2023 26th International Conference on Information Fusion (FUSION)*. IEEE, 2023, pp. 1–7.

[36] S. J. Julier and J. K. Uhlmann, "New extension of the Kalman filter to nonlinear systems," in *Signal Processing, Sensor Fusion, and Target Recognition VI*, vol. 3068. Spie, 1997, pp. 182–193.

[37] E. Mazor, A. Averbuch, Y. Bar-Shalom, and J. Dayan, "Interacting multiple model methods in target tracking: a survey," *IEEE Transactions on Aerospace and Electronic Systems*, vol. 34, no. 1, pp. 103–123, 2002.